RESEARCH ARTICLE

Check for updates

Noncovalent functionalization of Ti₃C₂Tₓ using cationic porphyrins with enhanced stability against oxidation†

Ti$_3$C$_2$T$_X$ using cationic porphyrins with enhanced stability against oxidation†

Shameel Thurakkal [ID] and Xiaoyan Zhang [ID] *

Ti$_3$C$_2$T$_X$, as the most explored MXenes, are a rising star among 2D materials due to their astonishing physicochemical properties. However, their practical applications remain extremely challenging because of chemical degradation into TiO$_2$ nanoparticles due to oxidation. Chemical functionalization is an effective way to improve their stability against oxidation and tune the physicochemical properties of 2D materials. In this paper, Ti$_3$C$_2$T$_X$ is noncovalently functionalized using two different cationic porphyrins and the two hybrids show good stabilities in water against oxidation. The electrostatic interactions between the cationic porphyrins and the Ti$_3$C$_2$T$_X$ nanosheets are confirmed by the changes in the zetapotential and the photophysical measurements. The hybrids show a red shifted Soret band of the porphyrins with a complete quenching of the fluorescence emission, which confirms the effective interactions and an energy/electron transfer between the porphyrins and the Ti$_3$C$_2$T$_X$ nanosheets. The exfoliated and functionalized Ti$_3$C$_2$T$_X$ are characterized using various microscopic and spectroscopic techniques. The two hybrids exhibit pH dependent release of cationic porphyrins particularly under acidic conditions. This study proposes a potentially useful strategy for the preparation of highly stable and functional MXenes towards promising applications in biomedicines, optoelectronics and sensors.

Introduction

MXenes are a series of two-dimensional transition metal carbides and nitrides with a general formula of M$_{n+1}$X$_n$T$_X$, where M is an early transition metal (Ti, V, Nb, *etc.*), X denotes for C and/or N, T$_X$ represents surface termination (–OH, –O, –F, *etc.*) and n = 1, 2, or 3.[1,2] These materials are synthesized by selective etching of an 'A' element (group 13 or 14 element) layer from their corresponding MAX phase.[3,4] Owing to their high electrical conductivity, hydrophilic surfaces, flexibility and transparency, large electrochemically active surfaces, tunable properties *via* compositional and structural modification, MXenes have attracted extensive attention in the research community and have been widely used in various applications including supercapacitors,[5–9] batteries,[10–14] electrocatalysis,[15–17] electrochromic devices,[18,19] field-effect transistors (FETs),[20] electromagnetic interference shielding[21] and biomedicines.[22]

Since the first discovery of MXenes in 2011, Ti$_3$C$_2$T$_X$ has been one of the most widely investigated MXenes.[23] The poor stability against oxidation of Ti$_3$C$_2$T$_X$ is a critical issue which hinders their practical applications.[24,25] The Ti$_3$C$_2$T$_X$ nanosheets gradually

Division of Chemistry and Biochemistry, Department of Chemistry and Chemical Engineering, Chalmers University of Technology, Kemigården 4, SE-412 96 Göteborg, Sweden. E-mail: xiaoyan.zhang@chalmers.se

† Electronic supplementary information (ESI) available. See DOI: 10.1039/d1qm01326b

degrade into TiO$_2$ nanoparticles in humid air or in water and lose their intrinsic physicochemical properties.[26,27] The ambient stability of Ti$_3$C$_2$T$_X$ nanosheets against oxidation can be improved by storing the water dispersions protected with argon at low temperatures.[24] Chemical functionalization has been recognized as an effective strategy to improve the ambient stability and the physicochemical properties of 2D materials.[28–37] Particularly, noncovalent functionalization can provide a higher degree of functionalization and largely preserve the intrinsic properties of 2D nanosheets to a great extent.[38] Chemically functionalized Ti$_3$C$_2$T$_X$ is expected to possess a higher stability against oxidation compared with the bare Ti$_3$C$_2$T$_X$ dispersions in water because of the presence of organic molecules or polymers at the surfaces, which can protect MXene nanosheets against oxidation by isolating the Ti atoms from oxygen. It has been reported that Ti$_3$C$_2$T$_X$ showed an improved stability in nonpolar organic media after surface modification with alkylphosphonic acids.[39] Kim and coworkers reported that the oxidation stability of MXene nanosheets can be enhanced by synthesizing Ti$_3$C$_2$T$_X$/polydopamine composites.[40] Different from these, it is anticipated that functional organic macrocyclic molecules with multiple positive charges can effectively interact with the functional groups of Ti$_3$C$_2$T$_X$ and noncovalently stack on the surface of MXenes to prevent it from oxidation.

Porphyrins are an important class of macrocyclic functional dyes with extraordinary physicochemical properties and hold potential applications in photomedicines,[41,42] and photovoltaic[43] and

optoelectronic devices.[44] Covalent or noncovalent functionalization of 2D materials such as graphene,[45–47] transition metal dichalcogenides,[48] and black phosphorus nanosheets[49] using various porphyrins has already been reported to achieve novel hybrid materials with multifunctional properties such as nonlinear optical properties, photoenergy conversion, photo/electrochemical sensing and photocatalytic/electrocatalytic properties.[50–52] In the light of these studies, we anticipate that the electron rich functional groups on MXene surfaces can effectively interact with positively charged porphyrins, which can decorate MXene with new functional properties and enhance its stability against oxidation. Herein, we have synthesized two porphyrin–$Ti_3C_2T_X$ hybrids based on two different cationic porphyrins and studied their stability against oxidation and the effect of pH on their interactions. The present study will further boost up the blossoming of MXene research towards chemically functionalized MXenes with functional moieties such as relevant molecules/polymers for biological and electronic applications.

Experimental

Materials

Ti_3AlC_2 was purchased from Forsman (purity 98%). LiF (99.995%), HCl ($\geq$37%), 5,10,15,20-tetrakis(1-methyl-4-pyridinio)porphyrin tetra(p-toluenesulfonate) (dye content 97%) and 5,10,15,20-tetrakis(4-trimethylammoniophenyl)porphyrin tetra(p-toluenesulfonate) (dye content 90%) were purchased from Sigma-Aldrich and were used as received.

Instruments

Zeta potential of the dispersions was analysed using Zetasizer Nano Zs (Malvern instruments UK). Thermogravimetric analysis (TGA) was carried out on a TGA 3+ star system (Mettler Toledo, Columbus, OH, USA) under N_2 flow (50 mL min^{-1}) at a ramp rate of 10 °C min^{-1}. Raman analysis was performed on a WITec alpha300 R confocal Raman microscopy system (excitation at 532 nm) and mean Raman spectra were obtained by averaging 400 point Raman spectra. X-Ray photoelectron spectroscopy (XPS) analysis was carried out on a PHI 5000 VersaProbe III Scanning XPS Microprobe and the spectra were processed using the PHI multiPak software. Scanning electron microscopy (SEM) was performed on a Quanta 200 FEG ESEM. Transmission electron microscopy (TEM) and HR-TEM were performed on a FEI Tecnai T20 instrument at an acceleration voltage of 200 kV. Attenuated total reflectance infrared (ATR-IR) spectra were recorded using a PerkinElmer Frontier Infrared Spectrometer with a GladiATR, diamond crystal design. UV-visible absorption spectra were recorded on a Varian Cary 50 Bio UV-visible spectrophotometer and fluorescence spectra were recorded on a Varian Cary Eclipse fluorescence spectrophotometer.

Preparation of $Ti_3C_2T_X$

The etchant was prepared by adding 12 M LiF to 2 mL of 9 M HCl and the mixture was stirred with a Teflon magnetic bar for 5 minutes in a polypropylene centrifuging tube. To this etchant,
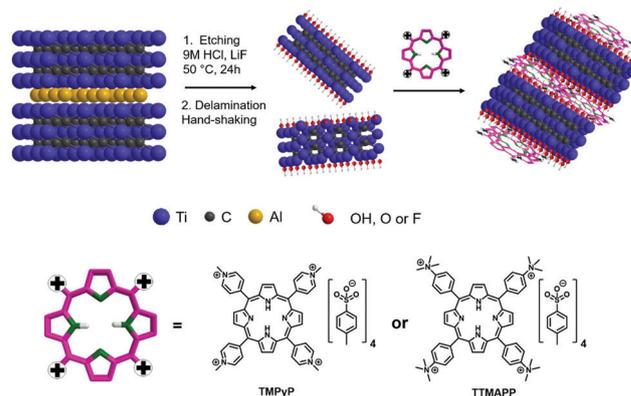
Scheme 1 Schematic illustration of the preparation of $Ti_3C_2T_X$ and its noncovalent functionalization using the cationic porphyrins, TMPyP and TTMAPP.

100 mg of Ti_3AlC_2 was slowly added and the mixture was stirred at 50 °C for 24 h. After stirring for 24 h, the etched solution was washed repeatedly with water by centrifuging at 4000 rpm for 10 minutes. At a pH of ∼5, delamination started. The dark green supernatant was collected by centrifuging at 4000 rpm for 10 minutes and the solid residues were stored as delaminated MXenes.

Preparation of $Ti_3C_2T_X$–porphyrin hybrids

The noncovalent functionalization of $Ti_3C_2T_X$ was carried out by gradually adding 3.6 mL of $Ti_3C_2T_X$ dispersion (0.6 mg mL^{-1}) into 75.56 mL of a TMPyP or a TTMAPP solution (3 μmol) in water and followed by shaking the mixture overnight. After shaking, almost all the solids were precipitated out with clear supernatants. The solids were separated by filtration using PTFE filter paper and the excess porphyrins were removed by gently washing the solids on the filter papers using water. The solid residues were dried under vacuum at 55 °C for 24 h and were directly used for further characterization studies.

Results and discussion

The $Ti_3C_2T_X$ was prepared by selective etching of Al from Ti_3AlC_2 using LiF and HCl at 50 °C and then by delamination using a hand shaking process (Scheme 1).[3] The as-prepared $Ti_3C_2T_X$ nanosheets appeared as a stable dispersion in water with a zetapotential value of −27.5 mV (Fig. S1, ESI†). This value indicates that the MXene surfaces are negatively charged possibly due to the presence of abundant electron rich hydroxyl, oxides and fluoride functional groups.[53] We have selected two different cationic porphyrins (with four positive charges on the peripheral groups) namely, 5,10,15,20-tetrakis(1-methyl-4-pyridinio)porphyrin tetra(p-toluenesulfonate) (TMPyP) and 5,10,15,20-tetrakis(4-trimethylammoniophenyl)porphyrin tetra(p-toluenesulfonate) (TTMAPP) for the functionalization of the $Ti_3C_2T_X$ (Scheme 1). The functionalization was carried out by titrating porphyrins with $Ti_3C_2T_X$ in deoxygenated water and followed by an overnight shaking using a shaker. After

562 | Mater. Chem. Front., 2022, 6, 561–569

This journal is © The Royal Society of Chemistry and the Chinese Chemical Society 2022

functionalization, the zetapotential was increased to +2.68 for the TMPyP–$Ti_3C_2T_X$ and −1.45 for the TTMAPP–$Ti_3C_2T_X$ and the two hybrids were precipitated out from water (Fig. S1, ESI†). The changes in the zetapotential confirm the effective electrostatic interactions between the positively charged porphyrin molecules and the $Ti_3C_2T_X$ surface. The TMPyP–$Ti_3C_2T_X$ and TTMAPP–$Ti_3C_2T_X$ hybrids were collected by centrifugation and dried under vacuum at 60 °C for 24 h.

The interactions between $Ti_3C_2T_X$ and the two cationic porphyrins were further investigated by analyzing the changes in the UV-visible absorption and fluorescence emission properties. The as-prepared $Ti_3C_2T_X$ dispersion in water showed the characteristic absorption peaks at ∼800 and 320 nm for the $Ti_3C_2T_X$.[54] The absorption spectra of the TMPyP showed a Soret band at 422 nm and Q bands at 518, 555, 584 and 640 nm, respectively, in water. The TTMAPP showed a Soret band at 412 nm and Q bands at 514, 550, 580 and 635 nm in water (Fig. S2 and S3, ESI†). A titration was performed by gradually adding the $Ti_3C_2T_X$ dispersion (0.2 mg mL^{-1}) into 1 μM solutions of the cationic porphyrins in water. For both the cationic porphyrins, the intensity of the Soret band was gradually decreased upon the addition of the $Ti_3C_2T_X$ dispersion. After adding 18 μg of the $Ti_3C_2T_X$, the Soret band of the free porphyrins was completely vanished with the formation of a new peak at 455 nm with a red shift of 33 nm for the TMPyP–$Ti_3C_2T_X$ and at 430 nm with a red shift of 18 nm for the TTMAPP–$Ti_3C_2T_X$. The red shift in the Soret band can be attributed to the flattening of porphyrins as the positively charged meso-groups can interact with the surface groups of the $Ti_3C_2T_X$ in the hybrids. In addition, the number and the intensities of the Q bands were found to be decreased after the formation of the hybrids, suggesting an increased symmetry of the cationic porphyrins due to their proximity on the $Ti_3C_2T_X$ surface (Fig. 1A and B).[55]

The fluorescence spectra of the TMPyP showed a relatively lower intensity emission peak at 680 nm and a higher intensity peak at 708 nm (Fig. S2, ESI†). Similarly, the TTMAPP exhibited a higher intensity emission peak at 643 nm and a lower intensity emission peak at 702 nm (Fig. S3, ESI†). In both cases, the addition of $Ti_3C_2T_X$ resulted in a complete quenching of the fluorescence, suggesting an effective electron and/or energy transfer between the cationic porphyrins and the $Ti_3C_2T_X$ (Fig. 1C–E). Similar observations were reported for other 2D and 1D nanomaterials including graphene,[45] MoS_2,[48] black phosphorus nanosheets[49] and carbon nanotubes.[56]

The morphology changes of $Ti_3C_2T_X$ during the preparation and functionalization were analyzed using SEM and TEM analysis. The Ti_3AlC_2 phase showed a densely stacked layer structure while the $Ti_3C_2T_X$ possessed a stacked layered morphology in the powder state (Fig. 2A and B). TEM images show the mono- to few-layer nanosheets of the $Ti_3C_2T_X$ by dropcasting its water dispersion onto a TEM grid (Fig. 2C). In addition, the high resolution TEM image confirms the crystalline nature of the synthesized $Ti_3C_2T_X$ (Fig. 2D). After the functionalization with porphyrin molecules, the $Ti_3C_2T_X$ nanosheets were found to be more aggregated which is in
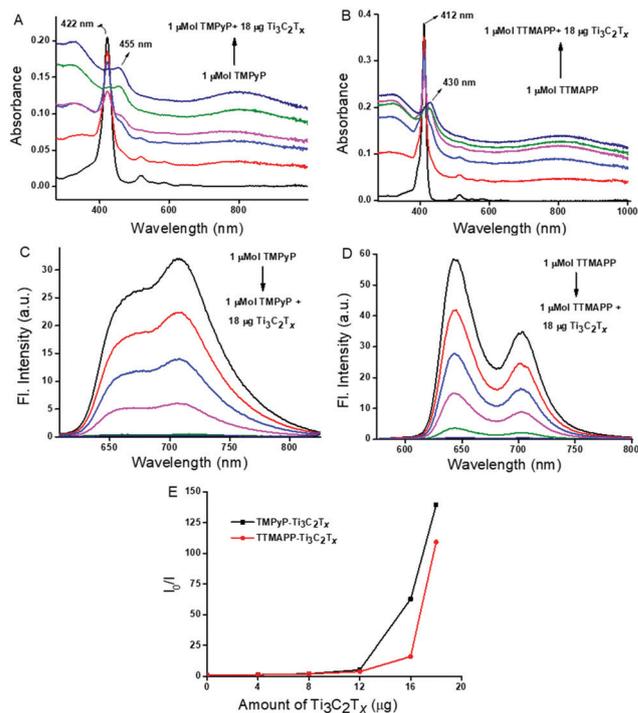

Fig. 1 Changes in the UV-visible absorption and fluorescence emission of 1 μM of TMPyP (A and C) and 1 μM of TTMAPP (B and D), upon titration with 0.2 mg mL^{-1} of $Ti_3C_2T_X$ in water, respectively. (E) The graph shows the extent of emission quenching with respect to the amount of the $Ti_3C_2T_X$ (I_0 and I are the intensity at fluorescence maxima of porphyrins before and after adding $Ti_3C_2T_X$, respectively).

accordance with the zetapotential changes and the aggregation in water (Fig. 2E and F).

XPS was used to study the chemical compositions and surface electronic states in the $Ti_3C_2T_X$ before and after functionalization. The survey spectra showed the presence of Ti, C, F, and O in all samples, while the presence of N was only found in the functionalized samples (Fig. S4, ESI†). The high resolution Ti2p, C1s, O1s and F1s XPS spectra of the bare $Ti_3C_2T_X$ are shown in the Fig. 3A–D. In the Ti2p XPS spectrum, the $2p_{3/2}$ peaks were located at 455.26, 456.19, 457.20, 458.45 and 459.61 eV, corresponding to the Ti–C, Ti^{2+}, Ti^{3+}, TiO_2 and Ti–F, respectively.[57] The C1s XPS spectrum can be fitted to five peaks at 281.94, 282.55, 284.84, 286.41 and 289.34 eV, assigned to the two C–Ti–T_X peaks, and C–C, C–O and C=O/C–F, respectively.[58,59] The O1s spectrum has been fitted to four peaks at 529.81, 530.68, 532.10 and 533.39 eV, attributed to the O–Ti (TiO_2), O–Ti (O/OH), O–C and adsorbed water molecules via hydrogen bonding to the terminal functional groups of the MXene.[59] The F1s spectrum showed two peaks at 685.24 and 686.77 eV, assigned to the F–Ti and F–C, respectively.[60] Fig. 3E and F show the high resolution Ti2p XPS spectra of the TMPyP–$Ti_3C_2T_X$ and the TTMAPP–$Ti_3C_2T_X$, respectively. Similar to the fitting for the bare $Ti_3C_2T_X$, the Ti2p spectra of both the hybrids were fitted with a higher degree of oxidation (higher intensity of the TiO_2 peak), probably due to the exposure to ambient atmosphere during the preparation and washing
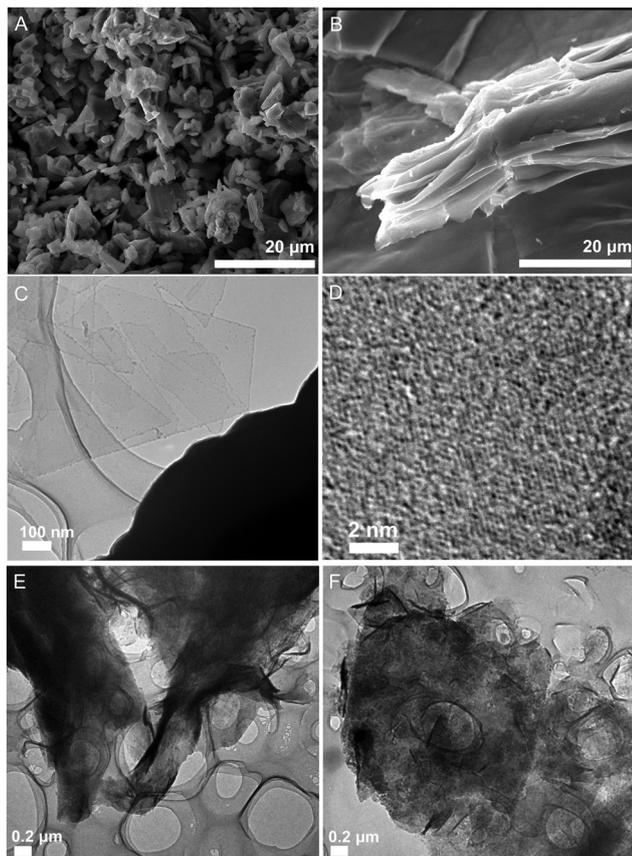
Fig. 2 SEM images of Ti_3AlC_2 (A) and $Ti_3C_2T_X$ (B) in the powder form. TEM image (C) and high-resolution TEM image (D) of $Ti_3C_2T_X$. TEM images of the TMPyP–$Ti_3C_2T_X$ (E) and the TTMAPP–$Ti_3C_2T_X$ (F).

processes. The N1s spectra of the hybrids show three peaks at 397.85, 399.67 and 401.76 eV for the TMPyP–$Ti_3C_2T_X$ (Fig. 3G) and at 397.45, 399.58 and 402.73 eV for the TTMAPP–$Ti_3C_2T_X$

(Fig. 3H), corresponding to the aza (–NH–), pyrrol (–C=N–) and peripheral pyridinium/quaternary ammonium nitrogen, respectively.[61]

TGA was performed under an N_2 atmosphere to study the thermal stability of the $Ti_3C_2T_X$ and the two hybrids (Fig. 4A). The $Ti_3C_2T_X$ showed a 2.6% weight loss from room temperature to 200 °C attributed to the adsorbed water molecules.[62] Another weight loss from 200–400 °C could be attributed to the decomposition of the OH and F functional groups. Apart from these, the hybrids showed a higher weight loss (around 5.5%) between 310 and 530 °C ascribed to the degradation of the porphyrins. Fig. 4B shows the mean Raman spectra of the $Ti_3C_2T_X$ and the hybrids, measured using a laser at an excitation wavelength of 532 nm. The $Ti_3C_2T_X$ showed several Raman bands: the one at 148 cm^{-1} is assigned to the Eg vibrational mode of anatase TiO_2,[63] the two bands at 260 and 403 cm^{-1} correspond to the Eg modes of the surface groups attached to Ti, and the band at 609 cm^{-1} is associated with the Eg vibrational modes of C.[64,65] The two peaks centered at 1341 and 1569 cm^{-1} are attributed to the D and G band of graphitic carbon, respectively.[66] After functionalization, the peak at 403 cm^{-1} was shifted to 426 cm^{-1} indicating the effective interactions between the cationic porphyrins and the surface functional groups of the $Ti_3C_2T_X$. Furthermore, ATR-IR spectra were recorded and the hybrids showed the C–H and C–N vibrational frequencies corresponding to the cationic porphyrins (Fig. S5, ESI†).

The stability of the $Ti_3C_2T_X$ and the hybrids against oxidation were studied and compared by investigating the changes in the absorption after storing the dispersions in undeoxygenated water at 5 °C for one week. Since the two hybrids were in the aggregated state in water, we have chosen the absorption peak at 260 nm corresponding to TiO_2 to track the oxidative degradation process, instead of using the $Ti_3C_2T_X$ characteristic peaks at 320 and 800 nm. After one week, the peak at 260 nm was found to be considerably increased in the case of the bare
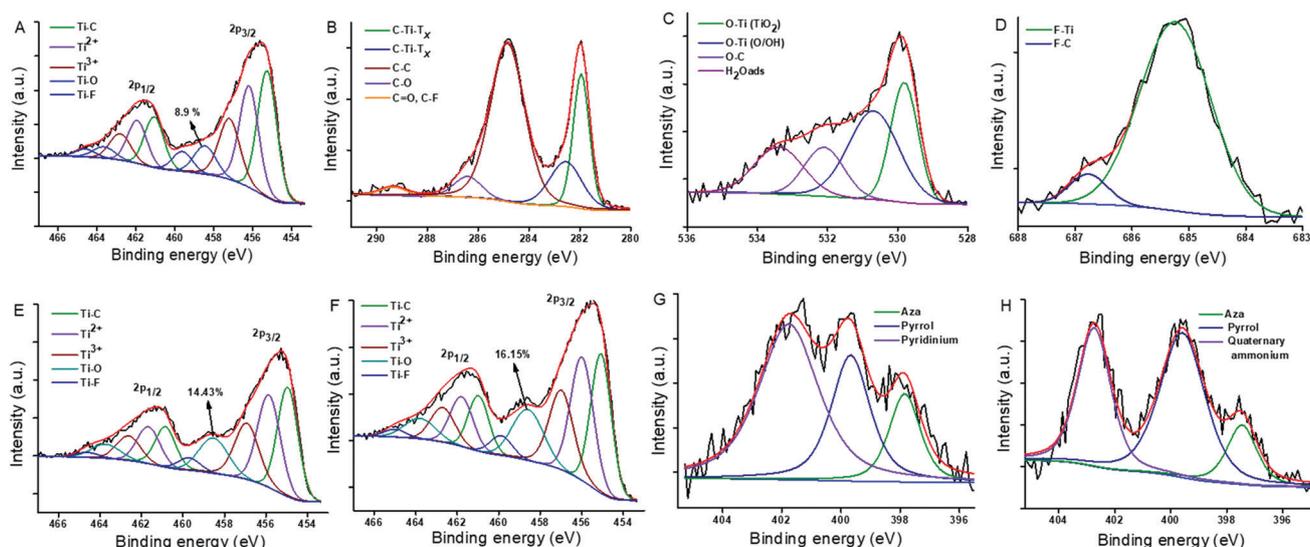

Fig. 3 High resolution Ti2p (A), C1s (B), O1s (C) and F1s (D) XPS spectra of $Ti_3C_2T_X$. High resolution Ti2p XPS spectra (E and F) and N1s spectra (G and H) of the TMPyP–$Ti_3C_2T_X$ and the TTMAPP–$Ti_3C_2T_X$, respectively.

564 | *Mater. Chem. Front.*, 2022, **6**, 561–569

This journal is © The Royal Society of Chemistry and the Chinese Chemical Society 2022
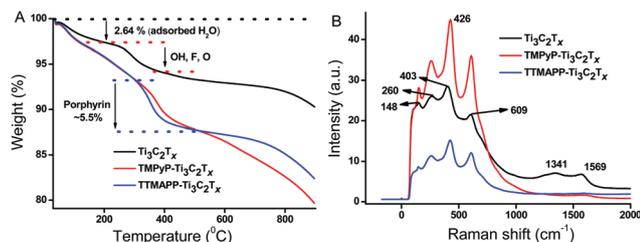
Fig. 4 TGA curves (A) and Raman spectra (B) of the $Ti_3C_2T_X$, TMPyP–$Ti_3C_2T_X$ and TTMAPP–$Ti_3C_2T_X$.

$Ti_3C_2T_X$ compared with those of the two hybrids, suggesting an improved stability against oxidation for the two hybrids (Fig. 5A–C). Moreover, the binding interactions between the $Ti_3C_2T_X$ and the cationic porphyrins were found to be highly stable because free porphyrins are not released in water even after one week. Furthermore, high resolution XPS was employed to confirm the improved stability against oxidation for the two hybrids. The Ti2p XPS spectra for the bare $Ti_3C_2T_X$ and the two hybrids were recorded after storing the samples for one week in undeoxygenated water (Fig. 5D–F) and the peak areas under Ti–O (TiO_2) region was compared with that of the spectra of the first day. After one week, the $Ti_3C_2T_X$ exhibited a vast increase of $\sim$104% in the intensity of the TiO_2 peak because of the fast degradation (Fig. S6, ESI†). In contrast, the TMPyP–$Ti_3C_2T_X$ and the TTMAPP–$Ti_3C_2T_X$ showed an increase of $\sim$21 and $\sim$6%, respectively, confirming that the noncovalent functionalization of the $Ti_3C_2T_X$ using the two cationic porphyrins resulted in a dramatic improvement of stability against oxidation in water.

Studying the effect of external stimuli like pH on the interactions between 2D materials and functional moieties in hybrid systems is highly important by considering both fundamental

research in term of interactions and also various applications aspects of such systems particularly biological applications in drug loading and releases at different pH values.[67,68] Since porphyrins are sensitive to the changes in pH, it is anticipated that the pH of the medium can tune the noncovalent interactions between the cationic porphyrins and the $Ti_3C_2T_X$ in the two hybrids. The free porphyrins exhibited different absorption and emission behavior with respect to the changes in pH due to the protonation or deprotonation of the porphyrins (Fig. S2 and S3, ESI†).[55] To study the effect of pH on the two hybrids, we have investigated the changes in the absorption and emission properties of the hybrids by varying the pH from neutral to both acidic and basic conditions. In the case of the TMPyP–$Ti_3C_2T_X$ hybrid, a peak at 422 nm corresponding to the free TMPyP was observed at pH 4. From pH 4 to pH 2, the intensity of the peak at 422 nm was found to be increased, suggesting an increased release of the free TMPyP from the hybrid (Fig. 6A). Correspondingly, we have observed an increase in the intensity of emission spectra as the pH decreases from 6 to 2 (Fig. 6B). The free TMPyP showed no obvious change in the absorption and emission until pH 2 (Fig. S2A, ESI†). At pH 4 and pH 2, the percentage of the TMPyP released from the TMPyP–$Ti_3C_2T_X$ hybrid was calculated to be 2.7% and 11.2%, respectively, based on the absorption intensity of the TMPyP at 422 nm. On the other hand, increasing pH to 12 did not have too much influence on the interaction as there was no remarkable absorption or emission peaks appeared corresponding to the free TMPyP (Fig. S7A and B, ESI†).

In the case of the TTMAPP–$Ti_3C_2T_X$ hybrid, no obvious peak for the free TTMAPP was observed until pH 5. At pH 4, an absorption peak at 412 nm corresponding to the free TTMAPP appeared (Fig. 6C). A slight increase in the emission intensity was observed from neutral to pH 5 and then a considerable increase at pH 4, suggesting a gradual release of the free
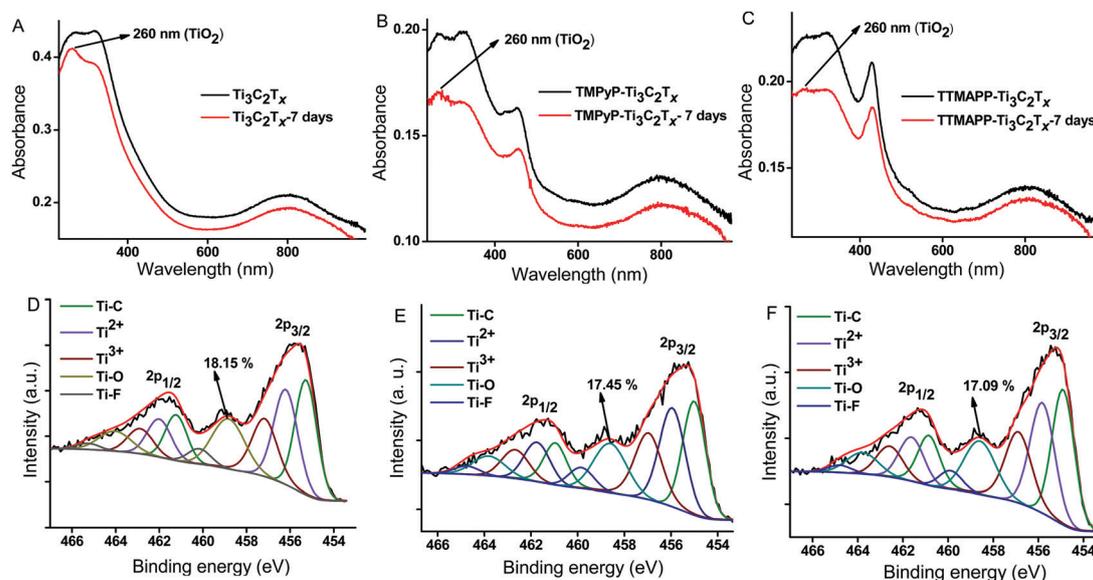

Fig. 5 Absorption changes (A–C) in water and Ti2p XPS spectra (D–F) of the $Ti_3C_2T_X$, TMPyP–$Ti_3C_2T_X$ and TTMAPP–$Ti_3C_2T_X$ after storing in water for one week.
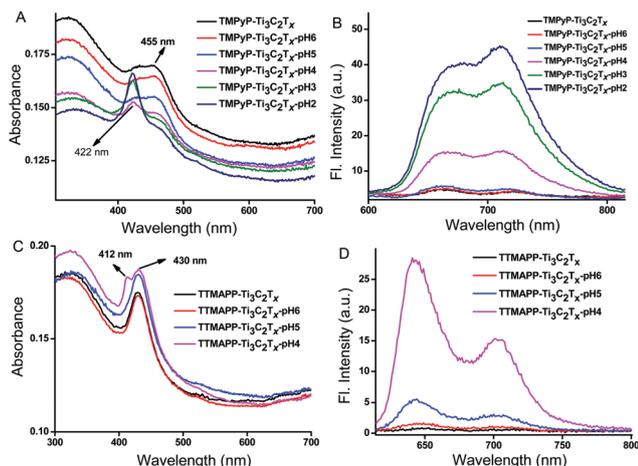
Fig. 6 Changes in the UV-visible absorption and fluorescence emission of the TMPyP–$Ti_3C_2T_X$ (A and B) and the TTMAPP–$Ti_3C_2T_X$ (C and D), respectively, under acidic conditions.

TTMAPP in water (Fig. 6D). Since the free TTMAPP shows a change in its absorption and emission structure at pH 3 due to protonation (Fig. S3A and B, ESI†), the effect of pH on the TTMAPP–$Ti_3C_2T_X$ was studied until pH 4. The percentage of the free TTMAPP released from the TTMAPP–$Ti_3C_2T_X$ hybrid at pH 4 is ~1.7%, which is lower than that of the TMPyP–$Ti_3C_2T_X$ hybrid released at the same pH, suggesting a stronger interaction in the case of the TTMAPP with the $Ti_3C_2T_X$. This observation further supports a higher stability against oxidation in the TTMAPP–$Ti_3C_2T_X$ hybrid compared with that of the TMPyP–$Ti_3C_2T_X$ hybrid in water. Furthermore, the pH of the hybrid dispersion was gradually increased to pH 12 and no peaks corresponding to the free TTMAPP were observed. However, a small increase in the emission intensity was seen from pH 9 to 12, indicating a slight release of the TTMAPP (Fig. S7C and D, ESI†). For both the hybrids, acidic conditions favor considerable release of the porphyrins compared with basic conditions. This can be attributed to the protonation of the functional groups present on the $Ti_3C_2T_X$ surface and consequently a lower interaction with the positively charged peripheral groups in the porphyrins.

Conclusions

In summary, $Ti_3C_2T_X$ was synthesized and noncovalently functionalized using two different cationic porphyrins. The electrostatic interactions between the $Ti_3C_2T_X$ and the porphyrins were studied by investigating the changes in the zetapotential and the photophysical properties. The exfoliated $Ti_3C_2T_X$ and the functionalized $Ti_3C_2T_X$ were further characterized using SEM, TEM, XPS, TGA and Raman analyses. The functionalized $Ti_3C_2T_X$ showed a largely improved stability against oxidation in water which was confirmed by UV-visible absorption measurement and high resolution XPS analyses. Finally, the effect of pH on the interactions between the $Ti_3C_2T_X$ and the cationic porphyrins was investigated and it was found that pH

dependent release of the porphyrins is possible especially under acidic conditions. This study will further fuel the growing research in MXenes and will serve as an example for chemical functionalization of MXenes using attractive functional molecules for applications towards drug loading and release,[69] nonlinear optical or optical limiting devices,[70] and photo- or electro-catalysis.[71,72]

Conflicts of interest

There are no conflicts to declare.

Acknowledgements

References

1 B. Anasori, M. R. Lukatskaya and Y. Gogotsi, 2D metal carbides and nitrides (MXenes) for energy storage, *Nat. Rev. Mater.*, 2017, **2**, 16098.

2 M. Naguib, V. N. Mochalin, M. W. Barsoum and Y. Gogotsi, 25th Anniversary Article: MXenes: A New Family of Two-Dimensional Materials, *Adv. Mater.*, 2014, **26**, 992–1005.

3 M. Alhabeb, K. Maleski, B. Anasori, P. Lelyukh, L. Clark, S. Sin and Y. Gogotsi, Guidelines for Synthesis and Processing of Two-Dimensional Titanium Carbide ($Ti_3C_2T_X$ MXene), *Chem. Mater.*, 2017, **29**, 7633–7644.

4 S. Yang, P. Zhang, F. Wang, A. G. Ricciardulli, M. R. Lohe, P. W. M. Blom and X. Feng, Fluoride-Free Synthesis of Two-Dimensional Titanium Carbide (MXene) Using A Binary Aqueous System, *Angew. Chem., Int. Ed.*, 2018, **57**, 15491–15495.

5 J. Yan, C. E. Ren, K. Maleski, C. B. Hatter, B. Anasori, P. Urbankowski, A. Sarycheva and Y. Gogotsi, Flexible MXene/Graphene Films for Ultrafast Supercapacitors with Outstanding Volumetric Capacitance, *Adv. Funct. Mater.*, 2017, **27**, 1701264.

6 Q. Jiang, Y. Lei, H. Liang, K. Xi, C. Xia and H. N. Alshareef, Review of MXene electrochemical microsupercapacitors, *Energy Storage Mater.*, 2020, **27**, 78–95.

7 W. Zhao, M. Jiang, W. Wang, S. Liu, W. Huang and Q. Zhao, Flexible Transparent Supercapacitors: Materials and Devices, *Adv. Funct. Mater.*, 2021, **31**, 2009136.

8 M. Ghidiu, M. R. Lukatskaya, M.-Q. Zhao, Y. Gogotsi and M. W. Barsoum, Conductive two-dimensional titanium carbide 'clay' with high volumetric capacitance, *Nature*, 2014, **516**, 78–81.

9 J. Pang, R. G. Mendes, A. Bachmatiuk, L. Zhao, H. Q. Ta, T. Gemming, H. Liu, Z. Liu and M. H. Rummeli,

This journal is © The Royal Society of Chemistry and the Chinese Chemical Society 2022

Applications of 2D MXenes in energy conversion and storage systems, *Chem. Soc. Rev.*, 2019, **48**, 72–133.

10 Q. Zhao, Q. Zhu, Y. Liu and B. Xu, Status and Prospects of MXene-Based Lithium–Sulfur Batteries, *Adv. Funct. Mater.*, 2021, **31**, 2100457.

11 Y. Xie, M. Naguib, V. N. Mochalin, M. W. Barsoum, Y. Gogotsi, X. Yu, K.-W. Nam, X.-Q. Yang, A. I. Kolesnikov and P. R. C. Kent, Role of Surface Structure on Li-Ion Energy Storage Capacity of Two-Dimensional Transition-Metal Carbides, *J. Am. Chem. Soc.*, 2014, **136**, 6385–6394.

12 O. Mashtalir, M. R. Lukatskaya, M.-Q. Zhao, M. W. Barsoum and Y. Gogotsi, Amine-Assisted Delamination of Nb2C MXene for Li-Ion Energy Storage Devices, *Adv. Mater.*, 2015, **27**, 3501–3506.

13 Y. Dong, H. Shi and Z.-S. Wu, Recent Advances and Promise of MXene-Based Nanostructures for High-Performance Metal Ion Batteries, *Adv. Funct. Mater.*, 2020, **30**, 2000706.

14 C. Wu, C. Huang, Z. Zhang, Y. Xie, Z. Gao and H. Wang, Bulk $Ti_3C_2T_X$ anodes for superior sodium storage performance: the unique role of O-termination, *Mater. Chem. Front.*, 2021, **5**, 2810–2823.

15 A. Liu, X. Liang, X. Ren, W. Guan, M. Gao, Y. Yang, Q. Yang, L. Gao, Y. Li and T. Ma, Recent Progress in MXene-Based Materials: Potential High-Performance Electrocatalysts, *Adv. Funct. Mater.*, 2020, **30**, 2003437.

16 H.-J. Liu and B. Dong, Recent advances and prospects of MXene-based materials for electrocatalysis and energy storage, *Mater. Today Phys.*, 2021, **20**, 100469.

17 S. Bai, M. Yang, J. Jiang, X. He, J. Zou, Z. Xiong, G. Liao and S. Liu, Recent advances of MXenes as electrocatalysts for hydrogen evolution reaction, *npj 2D Mater. Appl.*, 2021, **5**, 78.

18 P. Salles, D. Pinto, K. Hantanasirisakul, K. Maleski, C. E. Shuck and Y. Gogotsi, Electrochromic Effect in Titanium Carbide MXene Thin Films Produced by Dip-Coating, *Adv. Funct. Mater.*, 2019, **29**, 1809223.

19 G. Valurouthu, K. Maleski, N. Kurra, M. Han, K. Hantanasirisakul, A. Sarycheva and Y. Gogotsi, Tunable electrochromic behavior of titanium-based MXenes, *Nanoscale*, 2020, **12**, 14204–14212.

20 B. Xu, M. Zhu, W. Zhang, X. Zhen, Z. Pei, Q. Xue, C. Zhi and P. Shi, Ultrathin MXene-Micropattern-Based Field-Effect Transistor for Probing Neural Activity, *Adv. Mater.*, 2016, **28**, 3333–3339.

21 A. Iqbal, P. Sambyal and C. M. Koo, 2D MXenes for Electromagnetic Shielding: A Review, *Adv. Funct. Mater.*, 2020, **30**, 2000883.

22 H. Lin, Y. Chen and J. Shi, Insights into 2D MXenes for Versatile Biomedical Applications: Current Advances and Challenges Ahead, *Adv. Sci.*, 2018, **5**, 1800518.

23 M. Naguib, M. Kurtoglu, V. Presser, J. Lu, J. Niu, M. Heon, L. Hultman, Y. Gogotsi and M. W. Barsoum, Two-Dimensional Nanocrystals Produced by Exfoliation of Ti_3AlC_2, *Adv. Mater.*, 2011, **23**, 4248–4253.

24 C. J. Zhang, S. Pinilla, N. McEvoy, C. P. Cullen, B. Anasori, E. Long, S.-H. Park, A. Seral-Ascaso, A. Shmeliov, D. Krishnan, C. Morant, X. Liu, G. S. Duesberg, Y. Gogotsi and V. Nicolosi, Oxidation Stability of Colloidal Two-Dimensional Titanium Carbides (MXenes), *Chem. Mater.*, 2017, **29**, 4848–4856.

25 T. Habib, X. Zhao, S. A. Shah, Y. Chen, W. Sun, H. An, J. L. Lutkenhaus, M. Radovic and M. J. Green, Oxidation stability of $Ti_3C_2T_X$ MXene nanosheets in solvents and composite films, *npj 2D Mater. Appl.*, 2019, **3**, 8.

26 F. Xia, J. Lao, R. Yu, X. Sang, J. Luo, Y. Li and J. Wu, Ambient oxidation of Ti3C2 MXene initialized by atomic defects, *Nanoscale*, 2019, **11**, 23330–23337.

27 S. Huang and V. N. Mochalin, Hydrolysis of 2D Transition-Metal Carbides (MXenes) in Colloidal Solutions, *Inorg. Chem.*, 2019, **58**, 1958–1966.

28 S. Thurakkal and X. Zhang, Recent Advances in Chemical Functionalization of 2D Black Phosphorous Nanosheets, *Adv. Sci.*, 2020, **7**, 1902359.

29 S. Thurakkal, D. Feldstein, R. Perea-Causín, E. Malic and X. Zhang, The Art of Constructing Black Phosphorus Nanosheet Based Heterostructures: From 2D to 3D, *Adv. Mater.*, 2021, **33**, 2005254.

30 H. Huang, R. Jiang, Y. Feng, H. Ouyang, N. Zhou, X. Zhang and Y. Wei, Recent development and prospects of surface modification and biomedical applications of MXenes, *Nanoscale*, 2020, **12**, 1325–1338.

31 G. Zhang, T. Wang, Z. Xu, M. Liu, C. Shen and Q. Meng, Synthesis of amino-functionalized $Ti_3C_2T_X$ MXene by alkalization-grafting modification for efficient lead adsorption, *Chem. Commun.*, 2020, **56**, 11283–11286.

32 J. Kim, Y. Yoon, S. K. Kim, S. Park, W. Song, S. Myung, H.-K. Jung, S. S. Lee, D. H. Yoon and K.-S. An, Chemically Stabilized and Functionalized 2D-MXene with Deep Eutectic Solvents as Versatile Dispersion Medium, *Adv. Funct. Mater.*, 2021, **31**, 2008722.

33 V. Georgakilas, M. Otyepka, A. B. Bourlinos, V. Chandra, N. Kim, K. C. Kemp, P. Hobza, R. Zboril and K. S. Kim, Functionalization of Graphene: Covalent and Non-Covalent Approaches, Derivatives and Applications, *Chem. Rev.*, 2012, **112**, 6156–6214.

34 A. C. Ferrari, F. Bonaccorso, V. Fal'ko, K. S. Novoselov, S. Roche, P. Bøggild, S. Borini, F. H. L. Koppens, V. Palermo, N. Pugno, J. A. Garrido, R. Sordan, A. Bianco, L. Ballerini, M. Prato, E. Lidorikis, J. Kivioja, C. Marinelli, T. Ryhänen, A. Morpurgo, J. N. Coleman, V. Nicolosi, L. Colombo, A. Fert, M. Garcia-Hernandez, A. Bachtold, G. F. Schneider, F. Guinea, C. Dekker, M. Barbone, Z. Sun, C. Galiotis, A. N. Grigorenko, G. Konstantatos, A. Kis, M. Katsnelson, L. Vandersypen, A. Loiseau, V. Morandi, D. Neumaier, E. Treossi, V. Pellegrini, M. Polini, A. Tredicucci, G. M. Williams, B. Hee Hong, J.-H. Ahn, J. Min Kim, H. Zirath, B. J. van Wees, H. van der Zant, L. Occhipinti, A. Di Matteo, I. A. Kinloch, T. Seyller, E. Quesnel, X. Feng, K. Teo, N. Rupesinghe, P. Hakonen, S. R. T. Neil, Q. Tannock, T. Löfwander and J. Kinaret, Science and technology roadmap for graphene, related two-dimensional crystals, and hybrid systems, *Nanoscale*, 2015, **7**, 4598–4810.

35 C. Backes, A. M. Abdelkader, C. Alonso, A. Andrieux-Ledier, R. Arenal, J. Azpeitia, N. Balakrishnan, L. Banszerus, J. Barjon, R. Bartali, S. Bellani, C. Berger, R. Berger, M. M. B. Ortega,

C. Bernard, P. H. Beton, A. Beyer, A. Bianco, P. Bøggild, F. Bonaccorso, G. B. Barin, C. Botas, R. A. Bueno, D. Carriazo, A. Castellanos-Gomez, M. Christian, A. Ciesielski, T. Ciuk, M. T. Cole, J. Coleman, C. Coletti, L. Crema, H. Cun, D. Dasler, D. De Fazio, N. Díez, S. Drieschner, G. S. Duesberg, R. Fasel, X. Feng, A. Fina, S. Forti, C. Galiotis, G. Garberoglio, J. M. García, J. A. Garrido, M. Gibertini, A. Gölzhäuser, J. Gómez, T. Greber, F. Hauke, A. Hemmi, I. Hernandez-Rodriguez, A. Hirsch, S. A. Hodge, Y. Huttel, P. U. Jepsen, I. Jimenez, U. Kaiser, T. Kaplas, H. Kim, A. Kis, K. Papagelis, K. Kostarelos, A. Krajewska, K. Lee, C. Li, H. Lipsanen, A. Liscio, M. R. Lohe, A. Loiseau, L. Lombardi, M. Francisca López, O. Martin, C. Martín, L. Martínez, J. A. Martin-Gago, J. Ignacio Martínez, N. Marzari, Á. Mayoral, J. McManus, M. Melucci, J. Méndez, C. Merino, P. Merino, A. P. Meyer, E. Miniussi, V. Miseikis, N. Mishra, V. Morandi, C. Munuera, R. Muñoz, H. Nolan, L. Ortolani, A. K. Ott, I. Palacio, V. Palermo, J. Parthenios, I. Pasternak, A. Patane, M. Prato, H. Prevost, V. Prudkovskiy, N. Pugno, T. Rojo, A. Rossi, P. Ruffieux, P. Samorì, L. Schué, E. Setijadi, T. Seyller, G. Speranza, C. Stampfer, I. Stenger, W. Strupinski, Y. Svirko, S. Taioli, K. B. K. Teo, M. Testi, F. Tomarchio, M. Tortello, E. Treossi, A. Turchanin, E. Vazquez, E. Villaro, P. R. Whelan, Z. Xia, R. Yakimova, S. Yang, G. R. Yazdi, C. Yim, D. Yoon, X. Zhang, X. Zhuang, L. Colombo, A. C. Ferrari and M. Garcia-Hernandez, Production and processing of graphene and related materials, *2D Mater.*, 2020, **7**, 022001.

36 G. He, S. Huang, L. F. Villalobos, J. Zhao, M. Mensi, E. Oveisi, M. Rezaei and K. V. Agrawal, High-permeance polymer-functionalized single-layer graphene membranes that surpass the postcombustion carbon capture target, *Energy Environ. Sci.*, 2019, **12**, 3305–3312.

37 H. Riazi, M. Anayee, K. Hantanasirisakul, A. A. Shamsabadi, B. Anasori, Y. Gogotsi and M. Soroush, Surface Modification of a MXene by an Aminosilane Coupling Agent, *Adv. Mater. Interfaces*, 2020, **7**, 1902008.

38 C. Peng and X. Zhang, Chemical Functionalization of Graphene Nanoplatelets with Hydroxyl, Amino, and Carboxylic Terminal Groups, *Chemistry*, 2021, **3**, 873–888.

39 D. Kim, T. Y. Ko, H. Kim, G. H. Lee, S. Cho and C. M. Koo, Nonpolar Organic Dispersion of 2D $Ti_3C_2T_X$ MXene Flakes via Simultaneous Interfacial Chemical Grafting and Phase Transfer Method, *ACS Nano*, 2019, **13**, 13818–13828.

40 G. S. Lee, T. Yun, H. Kim, I. H. Kim, J. Choi, S. H. Lee, H. J. Lee, H. S. Hwang, J. G. Kim, D.-W. Kim, H. M. Lee, C. M. Koo and S. O. Kim, Mussel Inspired Highly Aligned $Ti_3C_2T_X$ MXene Film with Synergistic Enhancement of Mechanical Strength and Ambient Stability, *ACS Nano*, 2020, **14**, 11722–11732.

41 H. Huang, W. Song, J. Rieffel and J. F. Lovell, Emerging applications of porphyrins in photomedicine, *Front. Phys.*, 2015, **3**, 23.

42 M. Ethirajan, Y. Chen, P. Joshi and R. K. Pandey, The role of porphyrin chemistry in tumor imaging and photodynamic therapy, *Chem. Soc. Rev.*, 2011, **40**, 340–362.

43 L.-L. Li and E. W.-G. Diau, Porphyrin-sensitized solar cells, *Chem. Soc. Rev.*, 2013, **42**, 291–304.

44 C. B. Winkelmann, I. Ionica, X. Chevalier, G. Royal, C. Bucher and V. Bouchiat, Optical Switching of Porphyrin-Coated Silicon Nanowire Field Effect Transistors, *Nano Lett.*, 2007, **7**, 1454–1458.

45 Y. Xu, Z. Liu, X. Zhang, Y. Wang, J. Tian, Y. Huang, Y. Ma, X. Zhang and Y. Chen, A Graphene Hybrid Material Covalently Functionalized with Porphyrin: Synthesis and Optical Limiting Property, *Adv. Mater.*, 2009, **21**, 1275–1279.

46 D. Larowska, J. M. O'Brien, M. O. Senge, G. Burdzinski, B. Marciniak and A. Lewandowska-Andralojc, Graphene Oxide Functionalized with Cationic Porphyrins as Materials for the Photodegradation of Rhodamine B, *J. Phys. Chem. C*, 2020, **124**, 15769–15780.

47 D. Dasler, R. A. Schäfer, M. B. Minameyer, J. F. Hitzenberger, F. Hauke, T. Drewello and A. Hirsch, Direct Covalent Coupling of Porphyrins to Graphene, *J. Am. Chem. Soc.*, 2017, **139**, 11760–11765.

48 P. Jiang, B. Zhang, Z. Liu and Y. Chen, MoS2 quantum dots chemically modified with porphyrin for solid-state broadband optical limiters, *Nanoscale*, 2019, **11**, 20449–20455.

49 S. Thurakkal and X. Zhang, Covalent functionalization of two-dimensional black phosphorus nanosheets with porphyrins and their photophysical characterization, *Mater. Chem. Front.*, 2021, **5**, 2824–2831.

50 Y. Zhao, S. Ippolito and P. Samorì, Functionalization of 2D Materials with Photosensitive Molecules: From Light-Responsive Hybrid Systems to Multifunctional Devices, *Adv. Opt. Mater.*, 2019, **7**, 1900286.

51 Z.-B. Liu, Y.-F. Xu, X.-Y. Zhang, X.-L. Zhang, Y.-S. Chen and J.-G. Tian, Porphyrin and Fullerene Covalently Functionalized Graphene Hybrid Materials with Large Nonlinear Optical Properties, *J. Phys. Chem. B*, 2009, **113**, 9681–9686.

52 V. Georgakilas, J. N. Tiwari, K. C. Kemp, J. A. Perman, A. B. Bourlinos, K. S. Kim and R. Zboril, Noncovalent Functionalization of Graphene and Graphene Oxide for Energy Materials, Biosensing, Catalytic, and Biomedical Applications, *Chem. Rev.*, 2016, **116**, 5464–5519.

53 C. E. Ren, K. B. Hatzell, M. Alhabeb, Z. Ling, K. A. Mahmoud and Y. Gogotsi, Charge- and Size-Selective Ion Sieving Through $Ti_3C_2T_X$ MXene Membranes, *J. Phys. Chem. Lett.*, 2015, **6**, 4026–4031.

54 R. Li, L. Zhang, L. Shi and P. Wang, MXene Ti3C2: An Effective 2D Light-to-Heat Conversion Material, *ACS Nano*, 2017, **11**, 3752–3759.

55 E. Gacka, A. Wojcik, M. Mazurkiewicz-Pawlicka, A. Malolepszy, L. Stobiński, A. Kubas, G. L. Hug, B. Marciniak and A. Lewandowska-Andralojc, Noncovalent Porphyrin–Graphene Oxide Nanohybrids: The pH-Dependent Behavior, *J. Phys. Chem. C*, 2019, **123**, 3368–3380.

56 D. Baskaran, J. W. Mays, X. P. Zhang and M. S. Bratcher, Carbon Nanotubes with Covalently Linked Porphyrin Antennae: Photoinduced Electron Transfer, *J. Am. Chem. Soc.*, 2005, **127**, 6916–6917.

57 J. Halim, K. M. Cook, M. Naguib, P. Eklund, Y. Gogotsi, J. Rosen and M. W. Barsoum, X-ray photoelectron spectroscopy of select multi-layered transition metal carbides (MXenes), *Appl. Surf. Sci.*, 2016, **362**, 406–417.

This journal is © The Royal Society of Chemistry and the Chinese Chemical Society 2022

58 S. A. Shah, T. Habib, H. Gao, P. Gao, W. Sun, M. J. Green and M. Radovic, Template-free 3D titanium carbide ($Ti_3C_2T_X$) MXene particles crumpled by capillary forces, *Chem. Commun.*, 2017, **53**, 400–403.

59 J. Halim, M. R. Lukatskaya, K. M. Cook, J. Lu, C. R. Smith, L.-Å. Näslund, S. J. May, L. Hultman, Y. Gogotsi, P. Eklund and M. W. Barsoum, Transparent Conductive Two-Dimensional Titanium Carbide Epitaxial Thin Films, *Chem. Mater.*, 2014, **26**, 2374–2381.

60 L. Ding, Y. Wei, L. Li, T. Zhang, H. Wang, J. Xue, L.-X. Ding, S. Wang, J. Caro and Y. Gogotsi, MXene molecular sieving membranes for highly efficient gas separation, *Nat. Commun.*, 2018, **9**, 155.

61 J. P. Macquet, M. M. Millard and T. Theophanides, X-ray photoelectron spectroscopy of porphyrins, *J. Am. Chem. Soc.*, 1978, **100**, 4741–4746.

62 J. Li, X. Yuan, C. Lin, Y. Yang, L. Xu, X. Du, J. Xie, J. Lin and J. Sun, Achieving High Pseudocapacitance of 2D Titanium Carbide (MXene) by Cation Intercalation and Surface Modification, *Adv. Energy Mater.*, 2017, **7**, 1602725.

63 O. Frank, M. Zukalova, B. Laskova, J. Kürti, J. Koltai and L. Kavan, Raman spectra of titanium dioxide (anatase, rutile) with identified oxygen isotopes (16, 17, 18), *Phys. Chem. Chem. Phys.*, 2012, **14**, 14567–14572.

64 A. Sarycheva and Y. Gogotsi, Raman Spectroscopy Analysis of the Structure and Surface Chemistry of $Ti_3C_2T_X$ MXene, *Chem. Mater.*, 2020, **32**, 3480–3488.

65 T. B. Limbu, B. Chitara, M. Y. Garcia Cervantes, Y. Zhou, S. Huang, Y. Tang and F. Yan, Unravelling the Thickness Dependence and Mechanism of Surface-Enhanced Raman Scattering on $Ti_3C_2T_X$ MXene Nanosheets, *J. Phys. Chem. C*, 2020, **124**, 17772–17782.

66 M. Naguib, O. Mashtalir, M. R. Lukatskaya, B. Dyatkin, C. Zhang, V. Presser, Y. Gogotsi and M. W. Barsoum, One-step synthesis of nanocrystalline transition metal oxides on thin sheets of disordered graphitic carbon by oxidation of MXenes, *Chem. Commun.*, 2014, **50**, 7420–7423.

67 H. Zhang, T. Fan, W. Chen, Y. Li and B. Wang, Recent advances of two-dimensional materials in smart drug delivery nano-systems, *Bioact. Mater.*, 2020, **5**, 1071–1086.

68 X. Mei, T. Hu, Y. Wang, X. Weng, R. Liang and M. Wei, Recent advancements in two-dimensional nanomaterials for drug delivery, *Wiley Interdiscip. Rev.: Nanomed. Nanobiotechnol.*, 2020, **12**, e1596.

69 X. Yang, X. Zhang, Z. Liu, Y. Ma, Y. Huang and Y. Chen, High-Efficiency Loading and Controlled Release of Doxorubicin Hydrochloride on Graphene Oxide, *J. Phys. Chem. C*, 2008, **112**, 17554–17558.

70 J. W. You, S. R. Bongu, Q. Bao and N. C. Panoiu, Nonlinear optical properties and applications of 2D materials: theoretical and experimental aspects, *Nanophotonics*, 2019, **8**, 63–97.

71 J. Zhang, G. Chen, K. Müllen and X. Feng, Carbon-Rich Nanomaterials: Fascinating Hydrogen and Oxygen Electrocatalysts, *Adv. Mater.*, 2018, **30**, 1800528.

72 Z. You, Y. Liao, X. Li, J. Fan and Q. Xiang, State-of-the-art recent progress in MXene-based photocatalysts: a comprehensive review, *Nanoscale*, 2021, **13**, 9463–9504.